Research Article

Xin Zhang#, Xutong Zhu#, Lifa Huang, Zupeng Chen, Yuchen Wang*, Yajun Liu, Ruihan Pan, and Ling Lv*

Nano-encapsulated tanshinone IIA in PLGA-PEG-COOH inhibits apoptosis and inflammation in cerebral ischemia/reperfusion injury

https://doi.org/10.1515/gps-2022-8156
received December 27, 2022; accepted February 07, 2023

Abstract: Tanshinone IIA has a potential therapeutic effect on cerebral ischemia/reperfusion injury (CIRI). In this study, tanshinone IIA was encapsulated in poly (lactic-*co*-glycolic acid)-block-poly (ethylene glycol)-carboxylic acid (PLGA-PEG-COOH) nanoparticles, and its therapeutic efficacy on CIRI was investigated. Morphology and dynamic light scattering analyses were performed to identify and optimize nano-formulations. A drug release test was conducted using the dialysis method. The cytotoxic effect of tanshinone IIA on human neuroblastoma cells (SH-SY5Y) and brain endothelial capillary cells (hCMEC/D3) was measured using the MTT assay. The protective effect of PLGA-PEG-COOH-encapsulated tanshinone IIA against CIRI was evaluated in oxygen and glucose deprivation/reoxygenation-induced SH-SY5Y/IR cells and middle cerebral artery occlusion (MCAO) rats. Results showed that PLGA-PEG-COOH-encapsulated tanshinone IIA promoted viability and inhibited apoptosis of SH-SY5Y/IR cells ($P < 0.01$). Moreover, PLGA-PEG-COOH-encapsulated tanshinone IIA facilitated the invasion of SH-SY5Y/IR cells and repressed inflammation in MCAO rats ($P < 0.01$). Noteworthy, PLGA-PEG-COOH-encapsulated tanshinone IIA combined with angiopep-2 peptide presented a better inhibitory effect on CIRI than tanshinone IIA alone ($P < 0.01$). Angiopep-2 peptide contributes to traversing blood–brain barrier by recognizing lipoprotein-related protein expressed in the brain capillary endothelial cells. In conclusion, PLGA-PEG-COOH-encapsulated tanshinone IIA plus angiopep-2 peptide holds promising therapeutic potential toward CIRI.

Keywords: PLGA-PEG-COOH nanoparticles, tanshinone IIA, cerebral ischemia/reperfusion injury, angiopep-2 peptide, blood–brain barrier

1 Introduction

Cerebral ischemic, a common form of stroke, is mainly caused by blockage of a blood vessel due to a thrombus or embolus [1]. It affects all ages and is a leading cause of mortality and morbidity worldwide [2]. Several risk factors are associated with cerebral ischemic, including age, Fisher grade, tobacco smoking, systemic inflammatory response, diabetes, and obstructive hydrocephalus [2,3]. Tissue damage induced by cerebral ischemia is the main cause of fatal disease [4]. Early reperfusion is crucial for the recovery of blood flow in ischemic brain tissue but is not conducive to the recovery of brain function. In contrast, it further aggravates the dysfunction and structural damage caused by ischemia, known as cerebral ischemia/reperfusion injury (CIRI) [5–7]. The effects of neuronal necrosis, apoptosis, and poor prognosis after reperfusion during CIRI have been demonstrated [8–10].

# These authors have contributed equally to this work.

*** Corresponding author: Ling Lv,** Department of Neurosurgery, The First Affiliated Hospital of Zhejiang Chinese Medical University (Zhejiang Provincial Hospital of Chinese Medicine), No. 54, Youdian Road, Shangcheng District, Hangzhou 310006, Zhejiang, China, e-mail: lvlingiam@126.com
*** Corresponding author: Yuchen Wang,** Department of Neurosurgery, The First Affiliated Hospital of Zhejiang Chinese Medical University (Zhejiang Provincial Hospital of Chinese Medicine), No. 54, Youdian Road, Shangcheng District, Hangzhou 310006, Zhejiang, China, e-mail: edlefrei@163.com
Xin Zhang, Xutong Zhu, Lifa Huang, Zupeng Chen, Yajun Liu, Ruihan Pan: Department of Neurosurgery, The First Affiliated Hospital of Zhejiang Chinese Medical University (Zhejiang Provincial Hospital of Chinese Medicine), No. 54, Youdian Road, Shangcheng District, Hangzhou 310006, Zhejiang, China

It is of great significance to develop effective protection strategies and treatment methods for CIRI.

Oxidative stress and excessive inflammation are important pathophysiological mechanisms that cause neuronal apoptosis and brain injury after CIRI [11]. It has been proven that the clearance of excessive oxidative stress levels and regulation of the inflammatory microenvironment can slow down the process of neuronal death and improve prognosis [12,13]. Active components from traditional Chinese medicines possess favorable bioactivities including anti-oxidative stress, apoptosis, and inflammatory reactions [14,15]. Multi-component, multi-pathway, and multi-target features have unique therapeutic advantages and potential for CIRI with complex pathological mechanisms [16–19]. Tanshinones are lipophilic diterpenes isolated from the rhizome of *Salvia miltiorrhiza*, with favorable pharmacological activities against neurological diseases [20]. Tanshinone IIA is the mostly studied tanshinone, which reportedly mitigates blood–brain barrier (BBB) permeability in stroke [20]. It also reportedly exerts the therapeutic effect on CIRI. Song et al. suggested that tanshinone IIA modulates microglial polarization to confer anti-neuroinflammatory effects in CIRI [21]. Wang et al. demonstrated that sodium tanshinone IIA sulfonate protects against CIRI via inhibiting autophagy and inflammatory activity [22]. Tanshinone IIA also showed neuroprotective capabilities via anti-apoptotic pathway in rats with CIRI [23]. These previous studies confirmed the therapeutic efficacy of tanshinone IIA on CIRI.

Unfortunately, there are very few traditional Chinese medicine treatments that translate into clinical benefits [24–26]. The main reason may be that the rigidity of the BBB leads to ineffective drug delivery to the ischemic region, making it difficult to exert a therapeutic effect on the ischemic core [27–29]. As early as the 1970s, nanoparticles were first proposed as drug carriers and have been widely used in the field of biomedical transportation because of their biodegradability and sustained drug release [30–32]. Related studies have reported that puerarin-loaded poly(D,L-lactic-*co*-glycolic acid) nanoparticles increase and prolong puerarin concentration in the brain and promote functional recovery in ischemic regions [33]. We are aware of the BBB problem in the glioma area, and there have been many successful cases [34,35]. For example, studies on angiopep-2 peptide-functionalized nanoparticles demonstrated that compared with lactoferrin, transferrin, and avidin, the angiopep-2 peptide has a higher transport efficiency of BBB and glioma accumulation [36,37]. Moreover, it provides a proof of concept for lipoprotein receptor-related protein (LRP) receptor-mediated targeted administration in the cerebral ischemic region [38–40].

Poly(lactic-*co*-glycolic acid)-block-poly(ethylene glycol)-carboxylic acid (PLGA-PEG-COOH) constitutes the skeleton of the drug delivery nanoplatform [41]. Poly(lactic-*co*-glycolic acid) (PLGA) possesses good biodegradability and biocompatibility, which is a favorable shell for drug delivery [42]. Waters et al. suggested that tanshinone IIA-loaded PLGA nanoparticles mitigate neural injury in a translational pig ischemic stroke model [43]. Tanshinone IIA-loaded PEG-PLGA modified by borneol is a promising nose-to-brain delivery system that can enhance the prevention effect of tanshinone IIA on CIRI [44]. Herein, we designed multifunctional PLGA-PEG complex capsules with a water-soluble indocyanine green (ICG) fluorescent probe and ester-soluble tanshinone IIA by the water-in-oil-in-water (W/O/W) double emulsion method. Tanshinone IIA exhibits antiplatelet aggregation, antithrombotic activity, and improved microcirculation [45,46]. Angiopep-2 peptide modified by carboxyl on the surface of PLGA-PEG capsules can achieve the breakthrough of the BBB and targeted treatment of complex diseases (Scheme 1). The objective of the study was to achieve better targeted therapeutic effect of tanshinone IIA on CIRI by nanoparticle fabrication. This opens a new direction for the clinical treatment of CIRI and other oxidative stress-induced diseases.

2 Materials and methods

2.1 Materials

PLGA-PEG-COOH (MW = 10 K, PLGA: 75/25) was purchased from Ponsure Biotechnology Co., Ltd. (Shanghai, China). Poly(vinyl alcohol) (PVA) (88%, MW = 31,000) was obtained from Acros Organics (Geel, Belgium). Chloroform (AR) was purchased from Sinopharm Chemical Reagent Co., Ltd. (Shanghai, China). Tanshinone IIA (high-performance liquid chromatography [HPLC] ≥98%) was purchased from Yuanye Bio-Technology Co., Ltd. (Shanghai, China). Angiopep-2 peptide (TFFYGGSRGKRNNFKTEEYC) was obtained from China Peptides Co., Ltd. (Shanghai, China). ICG-Sulfo-Osu was purchased from Annoron Biotechnology Co., Ltd. (Beijing, China). Finally, 1-ethyl-3-(3-dimethylaminopropyl) carbodiimide hydrochloride (EDC) (99.9%) and *N*-hydroxysuccinimide (NHS) (99%) were provided by Aladdin Bio-Chem Technology Co., Ltd. (Shanghai, China).

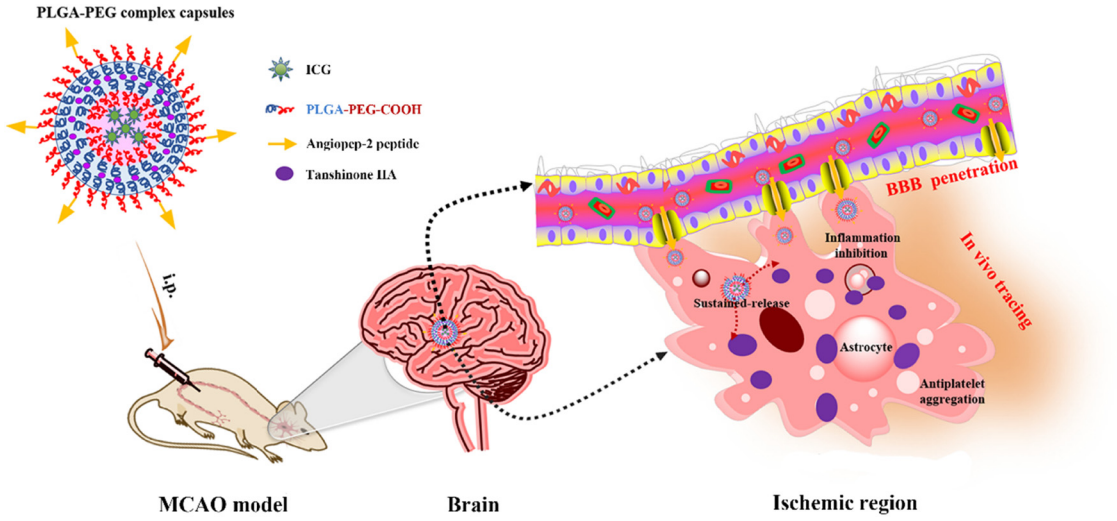

Scheme 1: PLGA-PEG-COOH-IT was selected for the preparation conditions and follow-up experiments.

2.2 Preparation of PLGA-PEG-COOH-ICG-tanshinone IIA (PLGA-PEG-COOH-IT) nanoparticles and PLGA-PEG complex capsules

PLGA-PEG-COOH-IT nanoparticles were fabricated by a typical double emulsion process (W/O/W). With 50 µL of ICG aqueous solution (4 mg·mL^{-1}) as the internal water phase, 1 mg tanshinone IIA and 50 mg PLGA-PEG-COOH were added to 1 mL chloroform. Colostrum was formed using an ultrasound probe for 30 s (80 W) in an ice bath. The colostrum was dripped into 3 mL of PVA (1% w/v, external water phase) and ultrasonicated with a probe for 2 min (80 W) in an ice bath to form a W/O/W double emulsion. Finally, the mixed solution was added to 50 mL of PVA (0.3% w/v, dispersed phase) and stirred overnight to volatilize the chloroform and solidify the nanosphere surface. Residual tanshinone IIA was removed by low-speed centrifugation (2,000 × *g*) for 7 min at 4°C. Then, ultrafiltration concentration and cleaning were performed at 4°C with a 100 kDa ultrafiltration tube to collect PLGA-PEG-COOH-IT nanoparticles. Finally, the collected PLGA-PEG-COOH-IT nanoparticles were stored at 4°C in pure water at a constant volume of 5 mL (10 mg·mL^{-1}). Appropriate samples were dried and weighed to determine their concentration and solid content. The non-loaded PLGA-PEG-COOH nanoparticles (without ICG and tanshinone IIA) were prepared using the same method.

LRP-targeted PLGA-PEG complex capsules were produced by a similar process. Briefly, 0.5 mL of PLGA-PEG-COOH-IT (10 mg·mL^{-1}) was dispersed in 1.5 mL of 4-morpholineethanesulfonic acid (MES) buffer (100 mM, pH 6.0; 100 µL MES buffer containing 10 mg EDC and 10 mg NHS) by shaking for 30 min at room temperature. Then, 5 mg angiopep-2 peptide (recognizing LRP) was poured into the reaction tube and shaken overnight. After coupling, the product was purified by ultrafiltration with pure water and stored in water. The ultrafiltered purified liquid was collected, and the coupling efficiency was determined.

2.3 Characterization of nanoparticles

The morphology of nanoparticles was examined by transmission electron microscopy (TEM) (JEM-2100, JEOL Ltd., Japan). The size and zeta potential of the nanoparticles were measured by dynamic light scattering (DLS) and Zetasizer Pro (Nano-ZS90, Malvern, UK). HPLC (Shimadzu, Japan) and UV-Vis absorption spectroscopy (UV-1780, Shimadzu, Japan) were used to determine drug release. The fluorescence spectrum and *in vitro* fluorescence imaging of nanoparticles were performed using a Fluoromax-4 spectrofluorometer (Horiba Scientific, Edison, NJ, USA) and an optical imaging system (IVIS Lumina LT, PerkinElmer, USA).

2.4 *In vitro* drug release

The release rate of tanshinone IIA from PLGA-PEG complex capsules *in vitro* was determined by a dialysis method. Briefly, 1 mL of PLGA-PEG complex capsule suspension was tightly placed into a centrifuge tube containing 5 mL

of sustained-release medium ([0.02 M phosphate-buffered saline, PBS, containing 1% SDS, pH 7.4 or 5.5]:methanol = 60:40) and put into a separate dialysis bag (MWCO: 8,000–14,000 Da). The centrifuge tube was then placed in a constant temperature shaker (120 rpm) at 37°C for continuous oscillation. At regular intervals (0, 0.5, 1, 2, 4, 19, 24, 48, 72, 96, and 120 h), 1 mL of dialysate was collected and filtered with a 0.45 μm membrane. Simultaneously, the filtered dialysate was replenished with an equal amount of the sustained-release medium to maintain constant volume. The released concentrations of tanshinone IIA at different time points were determined using HPLC at a wavelength of 270 nm. The cumulative release percentages of tanshinone IIA from nanoparticles were calculated.

2.5 CIRI cell model

SH-SY5Y (human neuroblastoma, CRL-2266), HaCaT (human immortalized keratinocytes, PCS-200-201), and hCMEC/D3 (human brain capillary endothelial, SCC066) cell lines were purchased from the ATCC (Manassas, VA, USA) and MilliPore (Bedford, MA, USA). H-SY5Y and HaCaT cells were cultured in the Dulbecco's modified Eagle's medium (DMEM; Gibco, Grand Island, NY, USA) added with 10% fetal bovine serum (FBS) and 1% sterile antibiotic–antimycotic solution. hCMEC/D3 cells were cultured in an EBM-2 medium (Lonza, Switzerland) containing 5% FBS, 1% penicillin/streptomycin, bFGF, hydrocortisone, and ascorbic acid. All these cells were incubated in a humidified atmosphere at 37°C with 5% CO_2. The SH-SY5Y cell model of CIRI (SH-SY5Y/IR) was established as previously reported by oxygen and glucose deprivation/reoxygenation (OGD/R) [47,48].

2.6 Cell viability and apoptosis assay

The effect of tanshinone IIA on the viability of SH-SY5Y and hCMEC/D3 cells was measured using the 3-(4,5-dimethylthiazol-2-yl)-2,5-diphenyltetrazolium bromide (MTT) assay. Cells were seeded in 96-well plates at 5×10^3 cells·well^{-1} and incubated for 24 h. Afterward, cells were incubated with tanshinone IIA (160 μg·mL^{-1}) for 24 h at 37°C. An equal volume of PBS was utilized as the control. Then, 20 μL of MTT reagent (5 mg·mL^{-1}; EMD Millipore, MA, USA) was added for further culture for 4 h, and dimethyl sulfoxide (100 μL·well^{-1}) was added to dissolve crystals. Absorbances of cells were measured by a Microplate Reader (Victor X, PerkinElmer, USA) at 570 nm.

For the CIRI cell model, SH-SY5Y cells were seeded in 12-well plates at 5×10^3 cells·well^{-1} and were incubated for 24 h. After washing with PBS, the cells were treated with different samples of tanshinone IIA (160 μg·mL^{-1}), PLGA-PEG-COOH (1.95 mg·mL^{-1}), PLGA-PEG-COOH-IT, and PLGA-PEG complex capsules (containing 160 μg·mL^{-1} tanshinone IIA) at 37°C for 24 h, and the PBS control group was set. Subsequently, cells were treated with OGD/R to induce CIRI. Cell viability was measured by the MTT assay as mentioned above. For apoptosis detection, the co-cultured cells were harvested, washed with ice-cold PBS, stained with the Annexin V-FITC/PI (Solarbio, CA1020, Beijing, China) for 15 min, and analyzed using flow cytometry (FACSCalibur, USA).

2.7 Cellular uptake behavior evaluation

The intracellular uptake of PLGA-PEG-COOH-IT and PLGA-PEG complex capsules was detected using a fluorescence microscope (Carl Zeiss Microscope Systems, Jena, Germany) [49], with PBS as the control. Briefly, SH-SY5Y cells were seeded on 6-well plates (1×10^5 cells·well^{-1}) the day before dosing and then incubated with complexes at 37°C for 6 h (OGD/R). Equivalent amounts of PBS buffer were used for comparison. The cells were washed and harvested. After fixation with 4% paraformaldehyde for 15 min, cell nuclei were labeled with 4′,6-diamidino-2-phenylindole (DAPI) for the same time. Finally, the fluorescence images were captured using a fluorescence microscope.

2.8 Hemocompatibility test

Fresh blood from healthy rats was stabilized with an anticoagulant (e.g., citrate dextrose), dispersed in PBS buffer (10%, v/v), and centrifuged for washing (1,500 rpm, 10 min) to obtain the supernatant. Diluted blood (0.2 mL) was added to each tube with different samples and incubated at 37°C for 1 h. Ultrapure water and PBS buffer were used as the positive (+Ref) and negative control groups (–Ref), respectively. After centrifugation, the supernatant was obtained by spectrophotometry (540 nm absorbance), and the hemolytic ratio (%) was calculated using the following formula [50]:

$$H(\%) = \frac{OD_{Sample} - OD_{-Ref}}{OD_{+Ref} - OD_{-Ref}} \times 100\% \quad (1)$$

2.9 Transwell invasion assay

To evaluate the potential of PLGA-PEG complex capsules penetrating the BBB, hCMEC/D3 cells were used to develop an *in vitro* model [51]. First, different drugs (PBS, tanshinone IIA, PLGA-PEG-COOH, PLGA-PEG-COOH-IT, and PLGA-PEG complex capsules) were added to the serum-free EBM-2 medium. The hCMEC/D3 cell (5×10^5 cells·mL^{-1}) in the above medium was seeded onto the upper chamber of the transwell insert containing a porous polycarbonate membrane (3 μm, Corning Costar, MD, USA) pre-coated with type I collagen. The medium containing 10% FBS was used as a chemoattractant in the lower chamber. After co-culturing for 48 h, SH-SY5Y/IR cells in the lower chamber of transwell were collected and washed three times with PBS. To verify the proliferation ability of SH-SY5Y/IR cells after treatment, we adopted the classic detection procedure mentioned in the previous literature [52]. The cells were stained with 0.1% crystal violet, observed, and counted under the microscope.

2.10 Western blotting (WB)

WB was performed to investigate the relative protein expression levels of LRP in SH-SY5Y, hCMEC/D3, and HaCaT cells. Cells cultured overnight were washed in PBS and lysed in 100 μL RIPA lysis buffer supplemented with a protease inhibitor cocktail (Sigma, P8340, MO, USA) to extract total proteins. Total proteins were separated by SDS-PAGE and incubated with an anti-LRP primary antibody (ab92544, 1:50; Abcam, UK) or GAPDH (ab8245, internal; Abcam) overnight at 4°C. After washing three times with Tris buffer and Tween, the blots were incubated with a secondary antibody for 1 h. Finally, ImageQuant LAS4000 Mini (GE Healthcare Life Science, Beijing, China) was used to detect the protein expression.

2.11 CIRI rat model and treatment

Sprague Dawley rats (Leagene, Bio-Technology Co., Ltd, Shanghai, China) were randomly divided into five groups (Sham, tanshinone IIA [10 mg·kg^{-1}], PLGA-PEG-COOH [100 mg·kg^{-1}], PLGA-PEG-COOH-IT, and PLGA-PEG complex capsules). Rats in each group were intraperitoneally injected with drug and nanoparticles containing 10 mg·kg^{-1} tanshinone IIA for seven consecutive days as previously reported [53]. The CIRI rat model was established by the middle cerebral artery occlusion (MCAO) operation. The bilateral common carotid artery was blocked by intraperitoneal injection of 10% chloral hydrate anesthesia (0.36 mL per 100 g) in rats after ischemia for 30 min. The clamp was removed, and blood reperfusion was restored for 90 min. During the experiment, the rats were kept at normal body temperature under a 100 W silk lamp (Guangqian Lighting Co., Ltd, Zhongshan, China). At the end of the experiment, rats were sacrificed by cervical dislocation. Brain tissues were immediately harvested, rinsed with cold saline, and kept at −80°C until use [54].

2.12 Distribution of nanoparticles in the brain homogenate

After intraperitoneal injection of PLGA-PEG-COOH-IT and PLGA-PEG complex capsules (tanshinone IIA: 10 mg·kg^{-1}) for 3 h, rats were euthanized, and brain tissues were collected for embedding, sectioning, and DAPI staining. The distribution of nanoparticles in brain tissues was observed under an inverted fluorescence microscope (Axio Observer.A1, ZEISS, Germany; excitation wavelength ICG = 780 nm and emission wavelength ICG = 845 nm).

2.13 Detection of inflammatory factor levels

Cortex tissues were placed in an ice-cold homogeneous buffer and centrifuged at 3,000 rpm to collect the supernatant. Levels of tumor necrosis factor-α (TNF-α), interleukin-6 (IL-6), and C-reactive protein (CRP) were determined using the corresponding enzyme-linked immunosorbent assay (ELISA) kits (FineTest, Wuhan, China).

2.14 Statistical analysis

Data in this study are represented as mean ± standard deviation. Student's *t*-test was performed to determine differences between two groups. Statistical significance was set at $P < 0.05$.

3 Results

3.1 Fabrication and characterization of nanoparticles

Nanoparticles were synthesized using the W/O/W double emulsion method. The size, zeta potential, fluorescence,

Table 1: Size, zeta-potential, fluorescence, and drug loading characteristics of the nanoparticles at different preparation parameters

Parameters	Nanoparticles				
	PLGA-PEG-COOH	PLGA-PEG-COOH-IT			
		1	2	3	4
Drug/ester ratio ($mg \cdot mg^{-1}$)	/	1:50	1:50	1:50	1:50
Oil/external water phase ($mL \cdot mL^{-1}$)	1:3	1:3	1:10	1:20	1:10
PLGA-PEG-COOH ($mg \cdot mL^{-1}$)	50	50	50	50	25
ICG (mg)	/	0.2	0.2	0.2	0.2
Tanshinone IIA (mg)	/	1	1	1	1.5
Z-Average (nm)	150.2	157	236.3	198.1	191.2
PDI	0.098	0.218	0.541	0.197	0.334
Zeta (mV)	−27.6	−30.5	−13.1	−14.2	−16.7
Fluorescence	/	Strong	Strong	Extremely weak	Weak
Encapsulation rate (%)	/	8.2	21.2	17.8	9.7
Drug loading (%)	/	0.23	0.38	0.29	0.45

and drug-loading characteristics of the nanoparticles at different preparation parameters are displayed in Table 1. Based on these parameters, PLGA-PEG-COOH-IT was selected as Scheme 1 for the preparation conditions and follow-up experiments. The morphology, particle size, and zeta potential of PLGA-PEG-COOH, PLGA-PEG-COOH-IT, and PLGA-PEG complex capsules were analyzed by TEM and Zetasizer Pro (Figure 1a–f). By comparing the TEM images in Figure 1a and c, it was found that the morphology of PLGA-PEG polymer nanoparticles changed significantly after drug loading, but the size changed less (approximately 100–150 nm). The surface potential changes of PLGA-PEG-COOH and PLGA-PEG-COOH-IT also confirmed the successful drug loading (Figure 1b and d). This was partly due to the negative charge on the ICG surface [55]. Based on the surface carboxyl-conjugated angiopep-2 peptide, the PLGA-PEG complex capsule spheres retained intact monodisperse nanospheres, showing a clear double-shell structure (Figure 1e). The particle size (~268.3 nm, PDI: 0.391) and zeta potential (~9.29 mV) were significantly different from those previously reported (Figure 1f). To some extent, the weakly positive surface charge reflects the anti-protein adsorption performance of the nanosystem during *in vivo* circulation [56].

3.2 *In vitro* fluorescence performance and drug release characteristics of nanoparticles

Nano-encapsulation water affinity of ICG as a near-infrared dye, with NIR-II fluorescence imaging performance, acts as a tracer in the body [57–59]. Therefore, it is necessary to verify the fluorescence properties of composite capsules *in vitro*. Compared with blank PLGA-PEG-COOH, the fluorescence spectra of PLGA-PEG-COOH-IT and PLGA-PEG complex capsules showed a prominent fluorescent signal between 820 and 850 nm (Figure 1g). This also confirmed that ICG was effectively encapsulated by nanoparticles. Fluorescence images in the illustration also revealed that the complex capsules still possessed high fluorescence ability and were unaffected by the modification.

To study the drug release characteristics, the tanshinone IIA release concentration in PLGA-PEG complex capsules was determined by HPLC (Figure 1h). As a biodegradable PLGA-PEG polymer material, tanshinone IIA is released slowly with its degradation [60,61]. From the release curve, tanshinone IIA has an obvious slow-release effect owing to its encapsulation in complex capsules. Only approximately 20% of drug release rate was achieved at pH 7.4, after 120 h. However, at pH 5.5, the release behavior was significantly different, reaching nearly 40% after 120 h. At the same time, the mass ratio (angiopep-2 peptide/tanshinone IIA) determined by HPLC was approximately 0.189.

3.3 LRP expression and *in vitro* cytotoxicity analysis of nanoparticles

To select suitable cell lines for subsequent *in vitro* function tests, we first measured the relative expression levels of LRP in SH-SY5Y, hCMEC/D3, and HaCaT cells by WB. WB analysis (Figure 2a) revealed that LRP was expressed in SH-SY5Y cells but not in hCMEC/D3 and HaCaT cells. To some extent, it was confirmed that modification of the angiopep-2 peptide based on the LRP target could improve the specific internalization behavior of target cells to nanodrugs, thus enhancing cell lethality.

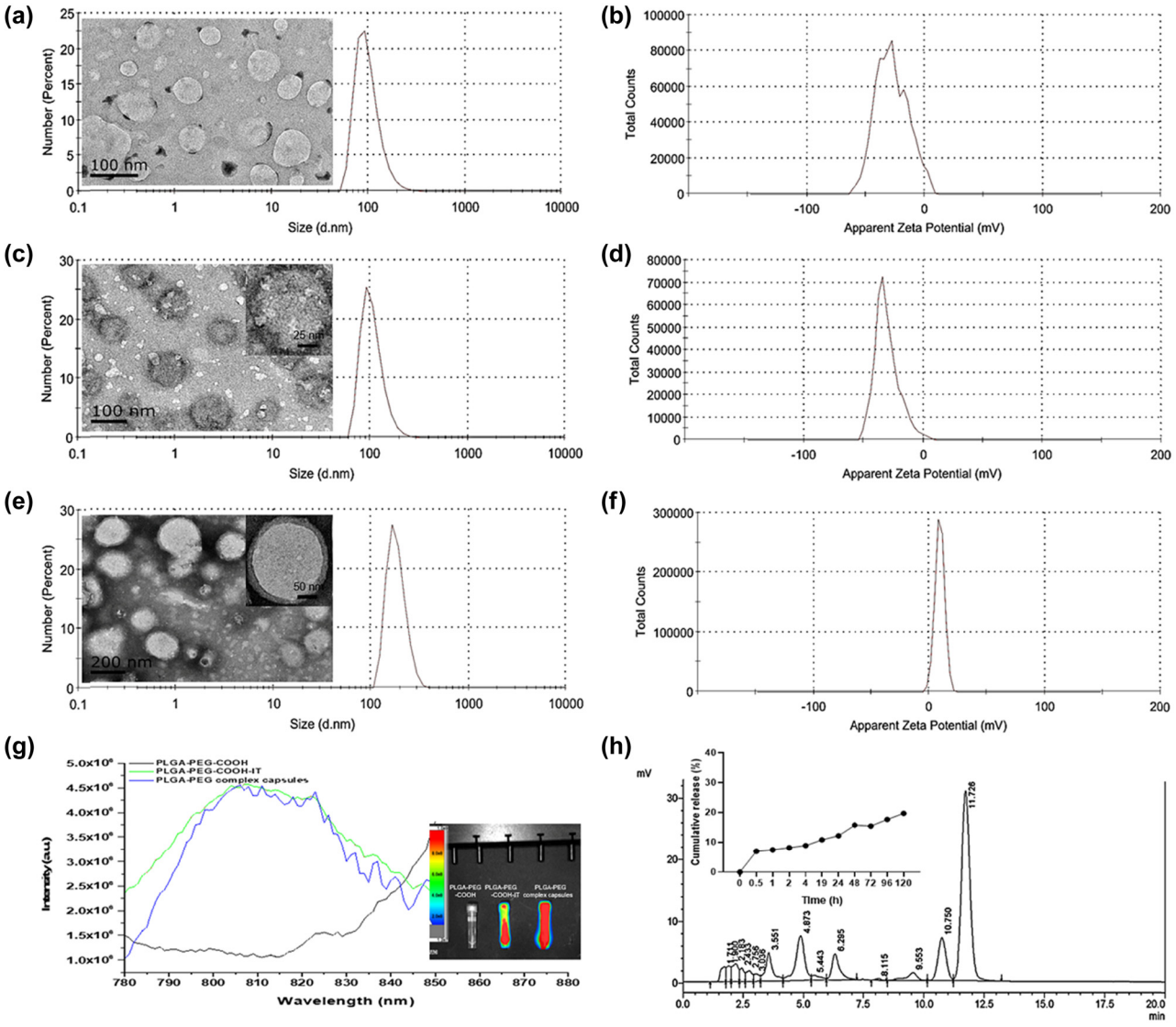

Figure 1: Characterization of PLGA-PEG complex capsules. TEM image, hydrodynamic size distribution, and zeta potential of PLGA-PEG-COOH (a and b), PLGA-PEG-COOH-IT (c and d), and PLGA-PEG complex capsules (e and f). (g) Fluorescence spectrum and fluorescence imaging (ICG excitation wavelength: 764 nm) of suspension samples. (h) HPLC chromatogram and *in vitro* release curve (pH 7.4 and 5.5) of tanshinone IIA.

The *in vitro* biocompatibility and CIRI therapeutic potential of PLGA-PEG complex capsules were studied in SH-SY5Y cells and SH-SY5Y/IR cells because they are easy to culture and have a common *in vitro* neuron model [48,62]. First, the effects of PLGA-PEG complex capsules on SH-SY5Y and hCMEC/D3 cell viability were evaluated (Figure 2b). The MTT assay demonstrated a dose-dependent decrease in cell viability ($P < 0.05$), but PLGA-PEG complex capsules did not induce any obvious cytotoxicity at tanshinone IIA concentrations up to 160 $\mu g \cdot mL^{-1}$. In this study, the effects of PBS, tanshinone IIA, PLGA-PEG-COOH, PLGA-PEG-COOH-IT, and PLGA-PEG complex capsules on the viabilities of SH-SY5Y/IR cells were further evaluated (Figure 2c). Compared with the control group, other groups containing tanshinone IIA had higher cell viability ($P < 0.01$). As expected, the nano-polymer capsules protected against IR-induced cell damage. In addition, flow cytometry showed that tanshinone IIA significantly inhibited the ratio of cell apoptosis induced by IR injury ($P < 0.05$; Figure 2d and e). An approximately 10.6% increase in apoptosis was observed in the PLGA-PEG-COOH group compared with that in the control group ($P < 0.01$). The proportion of apoptotic cells in the PLGA-PEG-COOH-IT and PLGA-PEG complex capsule groups decreased significantly (8.16 ± 0.33% and 2.43 ± 0.31%, respectively; $P < 0.001$). These results suggest that tanshinone IIA might alleviate IR injury by inhibiting apoptosis.

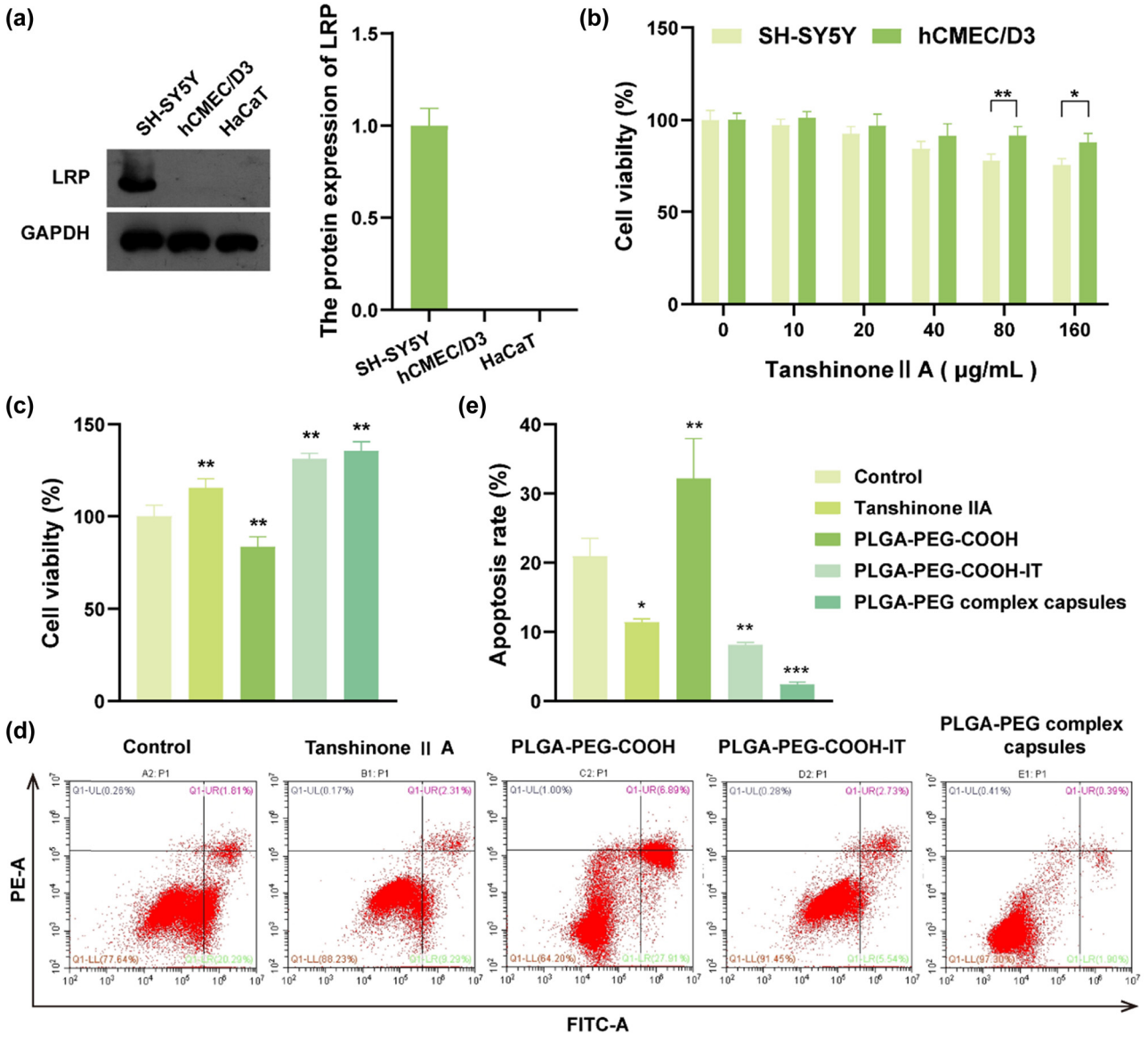

Figure 2: WB, cell viability, and apoptosis test *in vitro*. (a) LRP expressions in SH-SY5Y, hCMEC/D3, and HaCaT cells. (b) Effect of PLGA-PEG complex capsules with different dosages on SH-SY5Y and hCMEC/D3 cell viability ($n = 4$, mean ± SD, $^{*}P < 0.05$, $^{**}P < 0.01$). (c) Effects of different treatment groups on SH-SY5Y/IR cell viability co-incubated with nanoparticles before OGD/R treatment ($n = 4$, mean ± SD, $^{**}P < 0.01$). (d and e) Representative scatter plots and statistical histogram showing apoptosis in SH-SY5Y/IR cells by flow cytometry ($n = 3$, mean ± SD, $^{*}P < 0.05$, $^{**}P < 0.01$, $^{***}P < 0.001$).

3.4 *In vitro* intracellular distribution and the transportation of nanoparticles across BBB

The internalization behavior of cells to nanomedicine was further verified at the cellular level. In this study, the uptake of PLGA-PEG-COOH-IT and PLGA-PEG complex capsules by SH-SY5Y/IR cells was observed by fluorescence microscopy (Figure 3). Compared with the control group, a certain amount of ICG green fluorescence appeared in cells treated by PLGA-PEG-COOH-IT, indicating that some nanoparticles were successfully ingested by cells. Comparatively, the green fluorescence intensity in the PLGA-PEG complex capsules group was the most significant, indicating that angiopep-2 peptide as a specific ligand of LRPs might promote the uptake of nanoparticles [63].

Additional evidence to support this hypothesis was based on the transwell BBB model test *in vitro*. The BBB model was first established using monolayers of hCMEC/D3 cells cultured on a transwell insert with an aperture of 3 μm (Figure 4a and b). The activity of

SH-SY5Y/IR cells in the lower chamber was detected to evaluate the ability of nanocomposite capsules to break through the BBB. Compared with other groups, PLGA-PEG complex capsule treatment significantly improved the ability of SH-SY5Y/IR cells to break through the BBB ($P < 0.001$). Compared with the control group, the PLGA-PEG complex capsule group showed perfect cell proliferation ability ($P < 0.001$), similar to that in Figure 2c. However, the efficacy of free tanshinone IIA is not only offset by passive diffusion and drug efflux in SH-SY5Y/IR cells but also by drug efflux mechanisms operating in hCMEC/D3 cells [51,64]. Our results confirmed the potential of PLGA-PEG complex capsules to deliver therapeutic drugs across the BBB *in vitro*.

3.5 Hemocompatibility of nanoparticles

Hemocompatibility detection in drug development research is used to observe whether the tested drug causes hemolysis and red blood cell coagulation [50]. Therefore, the biocompatibility of different nanoparticles was evaluated by a hemolysis assay after incubation for 60 min (Figure 4c and d). The pure tanshinone IIA group had a higher hemolysis rate ($P < 0.001$). The hemolysis rate decreased after the polymer nanoparticles were coated, and PLGA-PEG complex capsules were lower than PLGA-PEG-COOH-IT ($P < 0.01$). These results met the requirements for medical applications of biomaterials and indicated that the PLGA-PEG complex capsules had good biocompatibility.

3.6 *Ex vivo* distribution, inflammatory factor levels, and anti-ischemia–reperfusion efficacy in the MCAO rats

To evaluate the active targeting capability of angiopep-2 peptide-modified polymer nanoparticles toward the ischemic site in the rat brain, the MCAO rat model was developed as the research object [65]. PLGA-PEG-COOH-IT and PLGA-PEG

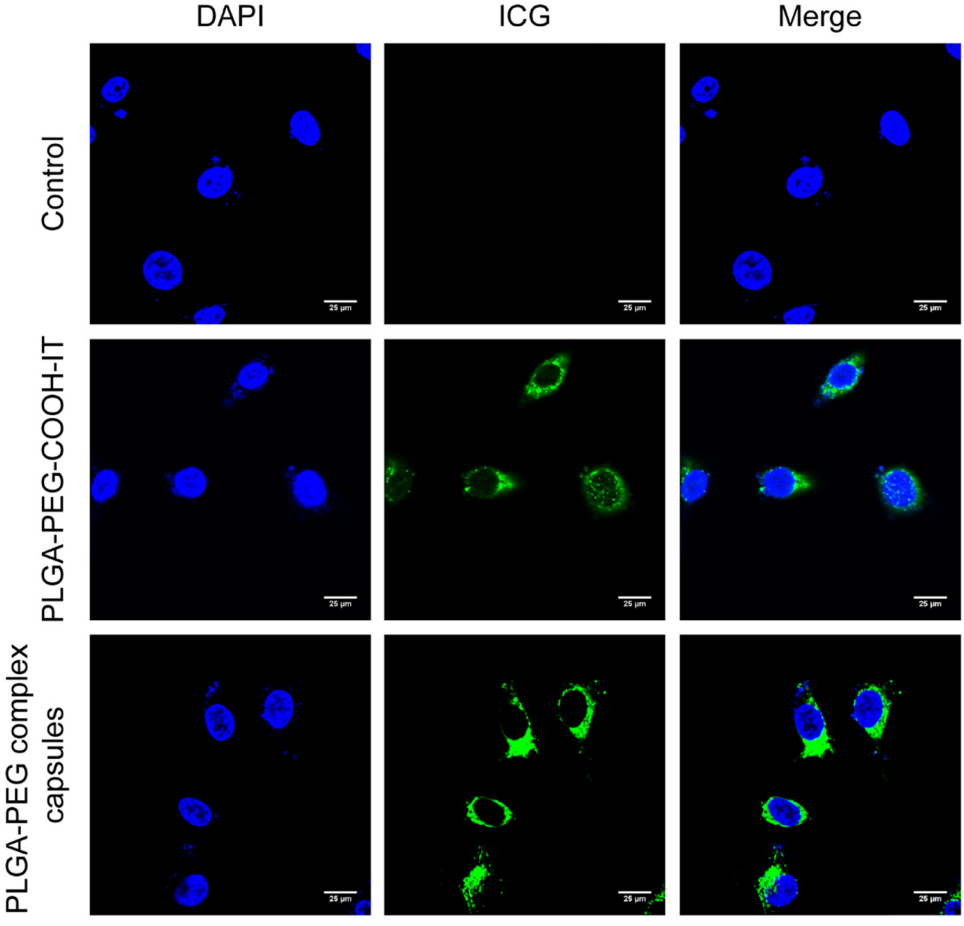

Figure 3: *In vitro* cellular internalization evaluation of PLGA-PEG-COOH-IT and PLGA-PEG complex capsules incubated with SH-SY5Y/IR cells for 6 h by fluorescence microscope (blue: cell nuclei; green: ICG; scale: 25 μm, $n = 3$).

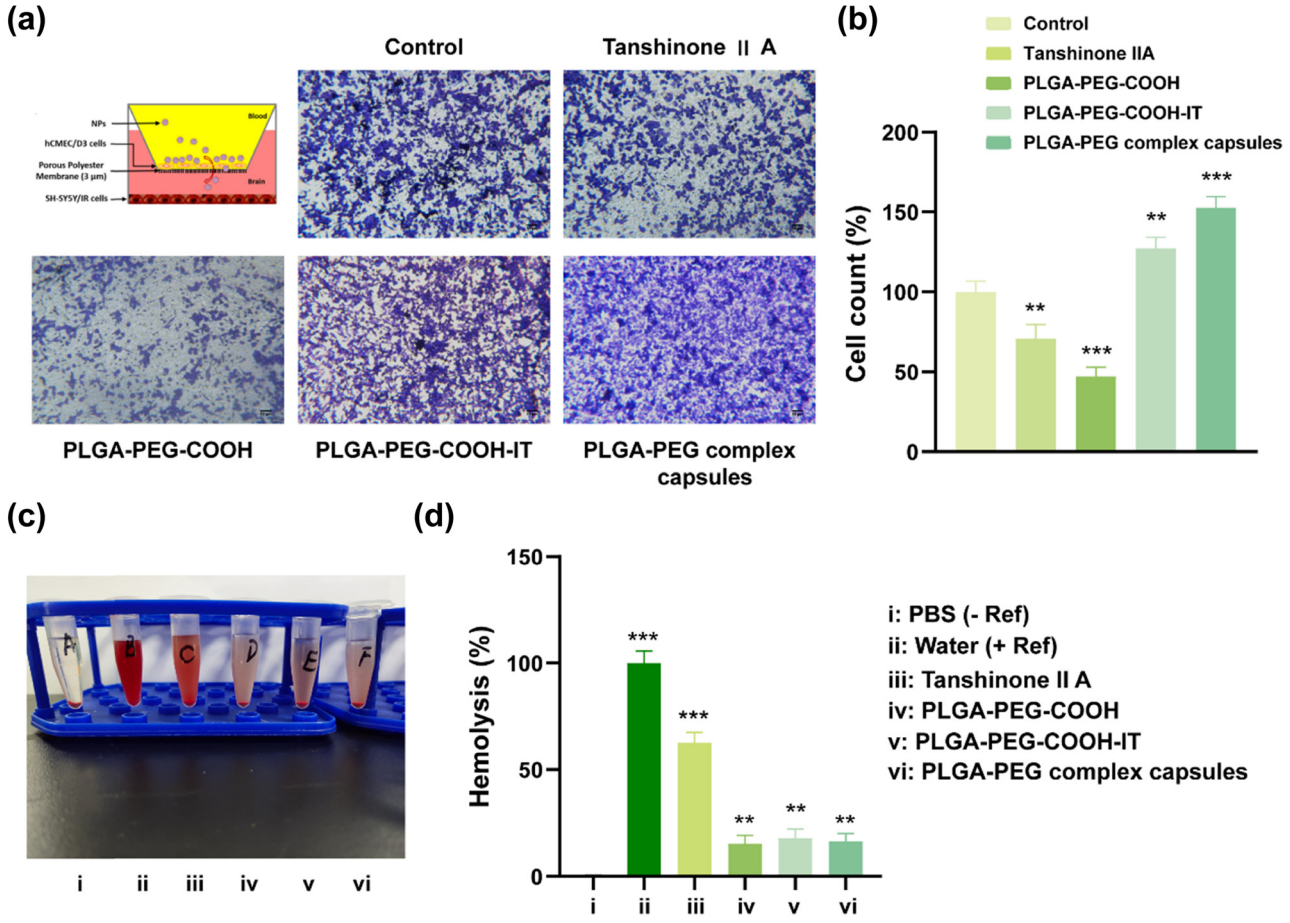

Figure 4: Evaluation of biological barrier-breaking and hemolytic activity *in vitro*. (a and b) Schematic of the *in vitro* BBB model formed by hCMEC/D3 cells over transwell insert with 3 μm pores. Proliferation was assessed at the 48-h treatment of stained SH-SY5Y/IR cells with crystal violet and viewing under an optical microscope, as well as evaluation of SH-SY5Y/IR cell number in the lower chamber of transwell BBB model after 48-h incubation (n = 3, mean ± SD, $^{**}P < 0.01$, $^{***}P < 0.001$). (c) Photographs of rat red blood cells after 60-min treatment with different samples: PBS (−Ref, 1), water (+Ref, 2), tanshinone IIA (3), PLGA-PEG-COOH (4), PLGA-PEG-COOH-IT (5), and PLGA-PEG complex capsules (6). (d) Graph summarizing the hemolytic activity of the corresponding groups (n = 3, mean ± SD, $^{**}P < 0.01$, $^{***}P < 0.001$).

complex capsules were injected intraperitoneally into MCAO rats. *Ex vivo* fluorescent imaging was performed on the ischemic cerebral homogenates of each group. The ICG green fluorescence intensity observed in the PLGA-PEG complex capsule groups was stronger than that of the sham and PLGA-PEG-COOH-IT groups ($P < 0.01$; Figure 5a and b). This indicates that the modification of the angiopep-2 peptide was conducive to the long circulation of nanoparticles and the accumulation of therapeutic drugs in the ischemic brain area. In general, the above results confirmed that the angiopep-2 peptide could actively enhance the targeting ability of nanoparticles to cerebral ischemia neurons. Also, the mechanism of angiopep-2 peptide homing to ischemic sites may be related to the overexpression of LRP in ischemic injury sites.

Meanwhile, the inflammatory responses at cerebral infarction sites in each group were explored. The ELISA test results in Figure 5c show that compared with other drug treatments in the MCAO model group, the treatment with PLGA-PEG complex capsules significantly decreased the levels of TNF-α, IL-6, and CRP ($P < 0.01$), indicating that the treatment could inhibit the inflammatory response of MCAO model mice. This result was consistent with the previous literature, reporting that tanshinone IIA could effectively alleviate cerebral ischemic injury [21]. More importantly, the treatment with PLGA-PEG-COOH-IT and PLGA-PEG complex capsules distinctly improved the neurological deficits induced by IR, indicating that tanshinone IIA exhibited greater neuroprotection than the other groups by nanoparticle encapsulation and angiopep-2 peptide functionalization. This study provided a novel approach to modify tanshinone IIA nanoparticles to elevate the ability of drug to cross the BBB [44].

4 Discussion

Over the past few decades, the branch of therapeutics based on complementary and alternative medicine has attracted considerable attention worldwide. The pharmacological efficacy of various traditional medicinal plants and their derivatives has been increasingly explored [66]. Tanshinone IIA, a fat-soluble diterpenoid isolated from *Salvia miltiorrhiza* Bunge, reportedly attenuates cerebral ischemic injury [21]. However, the low solubility and poor bioavailability of tanshinone IIA limit its clinical application. Nanoscale drug delivery systems are expected to produce synergistic anticancer effects, maximize therapeutic effects, and overcome multiple drug resistance [67]. The strategy of loading tanshinone IIA in nanoparticles may effectively improve the therapeutic efficacy of tanshinone IIA on CIRI. PLGA-PEG polymers have demonstrated their ability to improve traditional Chinese medicine preparations including tanshinone IIA [68,69]. However, it remains a challenge to increase the specific accumulation of drugs at injured sites and realize the controlled release of drugs in cells. In this study, tanshinone IIA was encapsulated in PLGA-PEG-COOH nanoparticles that were conjugated with ICG and angiopep-2 peptide. ICG is a water-soluble anionic tricarbocyanine dye mainly used for bioimaging applications [70]. Angiopep-2 peptide is a 19-mer peptide that can trigger transcytosis and traverse the BBB by recognizing LRP-1 expressed on the brain capillary endothelial cells [71]. After the characterization of the designed nanoparticles, the effects of tanshinone IIA-loaded PLGA-PEG-COOH nanoparticles were investigated on SH-SY5Y/IR cells and MCAO rats. Our results demonstrated that PLGA-PEG complex capsules loaded by tanshinone IIA, ICG, and angiopep-2 peptide can enhance the cellular uptake and attenuate CIRI *in vitro* and *in vivo*.

PLGA-PEG polymer nanoparticles can provide longer circulation times, thus enhancing drug localization at

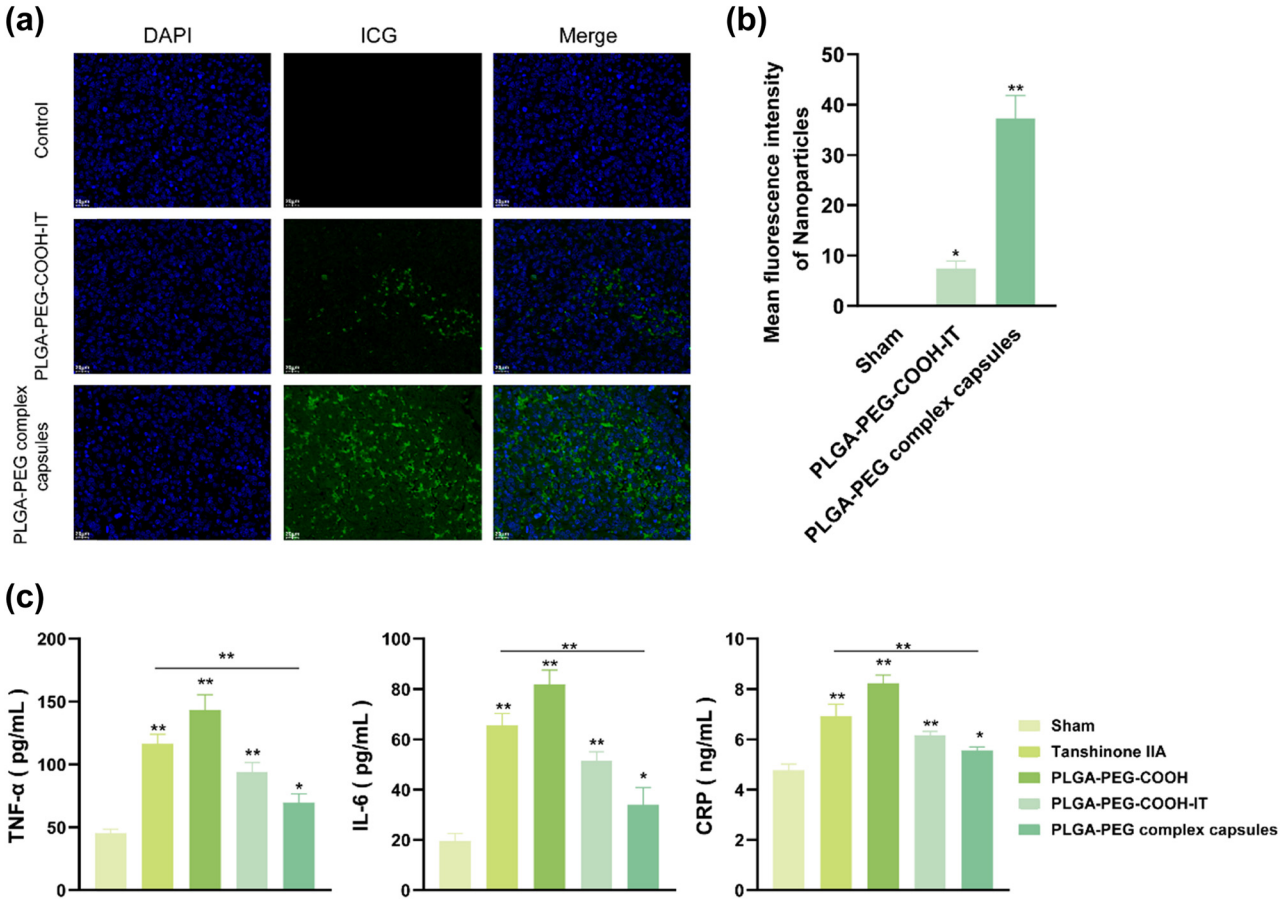

Figure 5: Distribution of nanoparticles and inflammatory response in brain tissues of the MCAO model. (a and b) Fluorescence distribution and intensity statistics ($n = 3$, $^{*}P < 0.05$, $^{**}P < 0.01$) of composite nanocapsules in the ischemic brain sections (DAPI blue fluorescence: cell nuclei; FITC green fluorescence: nanoparticle; scale: 20 μm). (c) The levels of TNF-α, IL-6, and CRP in the ischemic brain sections were detected by ELISA ($n = 3$).

the treatment site and selective targeting to improve the therapeutic index. However, the optimal properties also depend on the route of administration and the particle size of the nanocarrier. Nanoparticles with larger sizes show more retention upon local injection, and smaller sizes are more optimal for passive targeting [72]. Therefore, in this study, a series of attempts were made to prepare polyethylene–polyethylene glycol polymer nanoparticles with various excellent properties (Table 1). The prepared nanoparticles were characterized by TEM (nanoparticle shape) and DLS (hydrodynamic diameter and zeta potential) methods. Previous studies reported that nanoparticles have favorable physicochemical properties, contributing to cellular uptake and *in vivo* drug distribution [73,74]. In this study, the size and zeta potential of PLGA-PEG complex capsules were approximately 268.3 nm and 9.29 mV, respectively. Also, the PLGA-PEG polymer nanoparticles had a weak positive surface charge and spherical morphology, which to some extent reflects the anti-protein adsorption performance of the nanosystem during *in vivo* circulation [56]. In addition, the drug release of PLGA-PEG complex capsules was evaluated at pH 7.4 and pH 5.5. PLGA-PEG complex capsules showed a sustained-release pattern at pH 7.4, and just approximately 20% of drug release rate was achieved after 120 h. Such a sustained drug release may pertain to the electrostatic interaction between tanshinone IIA and nanoparticles. At pH 5.5, the drug release from PLGA-PEG complex capsules reached approximately 40% after 120 h, which may be owing to the loss of negative charge of nanoparticles.

Reliable diagnosis and effective targeted therapy are important; therefore, multifunctional nanotherapeutic agents show great potential for therapeutic and diagnostic applications in various diseases [75]. Interestingly, the fluorescence properties of drug delivery systems enable the simultaneous tracking and monitoring of drugs, which is very promising for drug delivery and targeted therapy [76]. Near-infrared (NIR)-responsive drug delivery systems have received enormous attention owing to their good biocompatibility and high biological penetration [77]. Among them, ICG has the dual function of *in vivo* fluorescence imaging and photoacoustic imaging, as well as the characteristic of single light-triggered nanoparticle-based phototherapies, which has an important potential for the future combined treatment of diseases [78]. Nano-encapsulation water affinity of ICG as a near-infrared dye, with NIR-II fluorescence imaging performance, acts as a tracer in the body [57–59]. Therefore, it is necessary to verify the fluorescence properties of the composite capsules *in vitro* and *in vivo*. The results showed that the synthesized PLGA-PEG polymer nanoparticles possessed excellent fluorescence and tracking properties *in vitro*.

Poor drug delivery for CIRI is a critical challenge in the treatment of ischemic stroke. Inspired by the intriguing BBB-penetrating ability of cancer cells upon their brain metastasis, promising biomimetic nanoplatforms targeting CIRI have been designed [27,79]. Israel synthesized a biodegradable nontoxic β-poly(L-malic acid) as a scaffold to chemically bind the BBB-crossing peptides such as angiopep-2 and MiniAp-4, and the transferrin receptor ligands such as cTfRL and B6 [80]. Angiopep-2-modified PLGA-PEG-based nanoparticles showed higher endocytosis and parenchymal accumulation, fully demonstrating targeted selectivity for receptor-mediated drugs in the brain [81]. This study further confirmed that PLGA-PEG complex capsules can be effectively taken up by SH-SY5Y/IR cells and break through the BBB.

Resistance and low drug efficacy have prompted the investigation of new therapeutic strategies that have high efficacy and low toxicity, especially for diseases with poor prognosis [82]. The MTT assay demonstrated that the PLGA-PEG complex capsules increased the viability of SH-SY5Y/IR cells and showed good biocompatibility. At the same time, PLGA-PEG complex capsules could effectively reverse CIRI, improve cell viability, and alleviate brain injury in animals at the cellular and animal levels. Of note, PLGA-PEG complex capsules presented better mitigative effect on CIRI than free tanshinone IIA or PLGA-PEG-COOH-IT.

5 Conclusion

This study successfully designed a promising tanshinone IIA-loaded PLGA-PEG polymer nanoparticle by combining the advantages of the nano-delivery system with the BBB-penetrating properties of the angiopep-2 peptide. We demonstrated that PLGA-PEG complex capsules can penetrate the BBB, deliver tanshinone IIA to the ischemic penumbra, and enhance its antioxidant and anti-inflammatory effects *in vivo*. The *in vitro* evaluation suggested that PLGA-PEG complex capsules might have the potential to provide greater protection against SH-SY5Y cytotoxicity in an IR-based model. In general, tanshinone IIA was encapsulated into PLGA-PEG-COOH nanoparticles loaded with ICG and angiopep-2 peptide, which contributes to traversing BBB and better drug release. Thus, tanshinone IIA could exert better therapeutic effect on CIRI. Consequently, PLGA-PEG complex capsules may be utilized as a potential delivery platform for tanshinone IIA to enhance the clinical treatment of CIRI. However, further investigations are required to confirm the therapeutic efficacy of PLGA-PEG complex

capsules on CIRI by animal and clinical experiments. Also, the specific cytotoxicity of PLGA-PEG complex capsules is needed to be evaluated.

Funding information: This work was supported by the National Natural Science Foundation of China (Grant number 81873186), and "Naoliuping" inhibits EMT and invasion and metastasis of glioblastoma through miRNAs-ZIC2 pathway mediated by DANCR and its mechanism (Grant number 2021ZZ011).

Author contributions: Xin Zhang: conceptualization, funding acquisition, writing – original draft; Xutong Zhu: conceptualization, writing – original draft; Lifa Huang: data curation, formal analysis; Zupeng Chen: data curation, methodology; Yuchen Wang: data curation, supervision; Yajun Liu: data curation, visualization; Ruihan Pan: data curation, validation; Ling Lv: conceptualization, writing – review and editing.

Conflict of interest: The authors state no conflict of interest.

Ethics statement: The study was reviewed and approved by the Animal Experiment Ethics Committee of The First Affiliated Hospital of Zhejiang Chinese Medical University.

Data availability statement: The data that support the findings of this study are available from the corresponding author upon reasonable request.

References

[1] Lee RHC, Lee MHH, Wu CYC, Couto ESA, Possoit HE, Hsieh TH, et al. Cerebral ischemia and neuroregeneration. Neural Regen Res. 2018;13(3):373–85.
[2] Dietz RM, Dingman AL, Herson PS. Cerebral ischemia in the developing brain. J Cereb Blood Flow Metab. 2022;42(10):1777–96.
[3] Rumalla K, Lin M, Ding L, Gaddis M, Giannotta SL, Attenello FJ, et al. Risk factors for cerebral vasospasm in aneurysmal subarachnoid hemorrhage: A population-based study of 8346 patients. World Neurosurg. 2021;145:e233–41.
[4] Zhu JJ, Yu BY, Huang XK, He MZ, Chen BW, Chen TT, et al. Neferine protects against hypoxic-ischemic brain damage in neonatal rats by suppressing NLRP3-mediated inflammasome activation. Oxid Med Cell Longev. 2021;2021:6654954.
[5] Mei ZG, Huang YG, Feng ZT, Luo YN, Yang SB, Du LP, et al. Electroacupuncture ameliorates cerebral ischemia/reperfusion injury by suppressing autophagy via the SIRT1-FOXO1 signaling pathway. Aging. 2020;12(13):13187–205.
[6] Yi X, Fang Q, Li L. MicroRNA-338-5p alleviates cerebral ischemia/reperfusion injury by targeting connective tissue growth factor through the adenosine 5'-monophosphate-activated protein kinase/mammalian target of rapamycin signaling pathway. Neuroreport. 2020;31(3):256–64.
[7] Liu D, Wang H, Zhang Y, Zhang Z. Protective effects of chlorogenic acid on cerebral ischemia/reperfusion injury rats by regulating oxidative stress-related Nrf2 pathway. Drug Des Dev Ther. 2020;14:51–60.
[8] Yan W, Sun W, Fan J, Wang H, Han S, Li J, et al. Sirt1-ROS-TRAF6 Signaling-induced pyroptosis contributes to early injury in ischemic mice. Neurosci Bull. 2020;36(8):845–59.
[9] Zuo G, Zhang D, Mu R, Shen H, Li X, Wang Z, et al. Resolvin D2 protects against cerebral ischemia/reperfusion injury in rats. Mol brain. 2018;11(1):9.
[10] Gu C, Yang H, Chang K, Zhang B, Xie F, Ye J, et al. Melatonin alleviates progression of uterine endometrial cancer by suppressing estrogen/ubiquitin C/SDHB-mediated succinate accumulation. Cancer Lett. 2020;476:34–47.
[11] Wang Y, Luo J, Li SY. Nano-curcumin simultaneously protects the blood-brain barrier and reduces m1 microglial activation during cerebral ischemia-reperfusion injury. ACS Appl Mater Interfaces. 2019;11(4):3763–70.
[12] Li C, Zhao Z, Luo Y, Ning T, Liu P, Chen Q, et al. Macrophage-disguised manganese dioxide nanoparticles for neuroprotection by reducing oxidative stress and modulating inflammatory microenvironment in acute ischemic stroke. Adv Sci. 2021;8(20):e2101526.
[13] Fan S, Liu X, Wang Y, Ren X, Liu Y, Dong Y, et al. Thymus quinquecostatus Celak. ameliorates cerebral ischemia-reperfusion injury via dual antioxidant actions: Activating Keap1/Nrf2/HO-1 signaling pathway and directly scavenging ROS. Phytomed Int J Phytother Phytopharmacol. 2021;91:153673.
[14] Ye T, Meng X, Zhai Y, Xie W, Wang R, Sun G, et al. Gastrodin ameliorates cognitive dysfunction in diabetes rat model via the suppression of endoplasmic reticulum stress and NLRP3 inflammasome activation. Front Pharmacol. 2018;9:1346.
[15] Wang Y, Su Y, Lai W, Huang X, Chu K, Brown J, et al. Salidroside restores an anti-inflammatory endothelial phenotype by selectively inhibiting endothelial complement after oxidative stress. Inflammation. 2020;43(1):310–25.
[16] Ma C, Wang X, Xu T, Yu X, Zhang S, Liu S, et al. Qingkailing injection ameliorates cerebral ischemia-reperfusion injury and modulates the AMPK/NLRP3 inflammasome signalling pathway. BMC Complementary Altern Med. 2019;19(1):320.
[17] Han JY, Li Q, Ma ZZ, Fan JY. Effects and mechanisms of compound Chinese medicine and major ingredients on microcirculatory dysfunction and organ injury induced by ischemia/reperfusion. Pharmacol Ther. 2017;177:146–73.
[18] Li L, Yang N, Nin L, Zhao Z, Chen L, Yu J, et al. Chinese herbal medicine formula tao hong si wu decoction protects against cerebral ischemia-reperfusion injury via PI3K/Akt and the Nrf2 signaling pathway. J Nat Med. 2015;69(1):76–85.
[19] Shi QH, Xiang J, Zhu XY, Cai DF. Protective effects of Chinese herbal medicine Naoshuantong on neurovascular unit in rats with cerebral ischemia/reperfusion injury. Zhong xi yi jie he xue bao = J Chin Integr Med. 2012;10(10):1135–9.
[20] Subedi L, Gaire BP. Tanshinone IIA: A phytochemical as a promising drug candidate for neurodegenerative diseases. Pharmacol Res. 2021;169:105661.
[21] Song Z, Feng J, Zhang Q, Deng S, Yu D, Zhang Y, et al. Tanshinone IIA protects against cerebral ischemia reperfusion

injury by regulating microglial activation and polarization via NF-kappaB pathway. Front Pharmacol. 2021;12:641848.
[22] Wang L, Xiong X, Zhang X, Ye Y, Jian Z, Gao W, et al. Sodium tanshinone IIA sulfonate protects against cerebral ischemia-reperfusion injury by inhibiting autophagy and inflammation. Neuroscience. 2020;441:46–57.
[23] Chen Y, Wu X, Yu S, Fauzee NJ, Wu J, Li L, et al. Neuroprotective capabilities of Tanshinone IIA against cerebral ischemia/reperfusion injury via anti-apoptotic pathway in rats. Biol Pharm Bull. 2012;35(2):164–70.
[24] Tang H, Pan CS, Mao XW, Liu YY, Yan L, Zhou CM, et al. Role of NADPH oxidase in total salvianolic acid injection attenuating ischemia-reperfusion impaired cerebral microcirculation and neurons: implication of AMPK/Akt/PKC. Microcirculation. 2014;21(7):615–27.
[25] Xie W, Zhu T, Zhou P, Xu H, Meng X, Ding T, et al. Notoginseng leaf triterpenes ameliorates OGD/R-induced neuronal injury via SIRT1/2/3-Foxo3a-MnSOD/PGC-1alpha signaling pathways mediated by the NAMPT-NAD pathway. Oxid Med Cell Longev. 2020;2020:7308386.
[26] Yang S, Wang H, Yang Y, Wang R, Wang Y, Wu C, et al. Baicalein administered in the subacute phase ameliorates ischemia-reperfusion-induced brain injury by reducing neuroinflammation and neuronal damage. Biomed Pharmacother = Biomed Pharmacother. 2019;117:109102.
[27] He W, Mei Q, Li J, Zhai Y, Chen Y, Wang R, et al. Preferential targeting cerebral ischemic lesions with cancer cell-inspired nanovehicle for ischemic stroke treatment. Nano Lett. 2021;21(7):3033–43.
[28] Bao Q, Hu P, Xu Y, Cheng T, Wei C, Pan L, et al. Simultaneous blood-brain barrier crossing and protection for stroke treatment based on edaravone-loaded ceria nanoparticles. ACS Nano. 2018;12(7):6794–805.
[29] Al-Ahmady ZS, Jasim D, Ahmad SS, Wong R, Haley M, Coutts G, et al. Selective liposomal transport through blood brain barrier disruption in ischemic stroke reveals two distinct therapeutic opportunities. ACS Nano. 2019;13(11):12470–86.
[30] Hong D, Song B, Kim H, Kwon J, Khang G, Lee D. Biodegradable polyoxalate and copolyoxalate particles for drug-delivery applications. Ther Delivery. 2011;2(11):1407–17.
[31] Zhang E, Xing R, Liu S, Qin Y, Li K, Li P. Advances in chitosan-based nanoparticles for oncotherapy. Carbohydr Polym. 2019;222:115004.
[32] Cao Y, Liu F, Chen Y, Yu T, Lou D, Guo Y, et al. Drug release from core-shell PVA/silk fibroin nanoparticles fabricated by one-step electrospraying. Sci Rep. 2017;7(1):11913.
[33] Tao HQ, Meng Q, Li MH, Yu H, Liu MF, Du D, et al. HP-beta-CD-PLGA nanoparticles improve the penetration and bioavailability of puerarin and enhance the therapeutic effects on brain ischemia-reperfusion injury in rats. Naunyn-Schmiedeberg's Arch Pharmacol. 2013;386(1):61–70.
[34] Lu Y, Han S, Zheng H, Ma R, Ping Y, Zou J, et al. A novel RGDyC/PEG co-modified PAMAM dendrimer-loaded arsenic trioxide of glioma targeting delivery system. Int J Nanomed. 2018;13:5937–52.
[35] Zhao M, Li A, Chang J, Fu X, Zhang Z, Yan R, et al. Develop a novel superparamagnetic nano-carrier for drug delivery to brain glioma. Drug Delivery. 2013;20(3–4):95–101.
[36] Han S, Zheng H, Lu Y, Sun Y, Huang A, Fei W, et al. A novel synergetic targeting strategy for glioma therapy employing borneol combination with angiopep-2-modified, DOX-loaded PAMAM dendrimer. J Drug Target. 2018;26(1):86–94.
[37] Qian W, Qian M, Wang Y, Huang J, Chen J, Ni L, et al. Combination glioma therapy mediated by a dual-targeted delivery system constructed using OMCN-PEG-Pep22/DOX. Small. 2018;14(42):e1801905.
[38] Hu L, Wang Y, Zhang Y, Yang N, Han H, Shen Y, et al. Angiopep-2 modified PEGylated 2-methoxyestradiol micelles to treat the PC12 cells with oxygen-glucose deprivation/reoxygenation. Colloids Surf B Biointerfaces. 2018;171:638–46.
[39] Wang X, Liu G, Chen N, Wu J, Zhang J, Qian Y, et al. Angiopep2-conjugated star-shaped polyprodrug amphiphiles for simultaneous glioma-targeting therapy and MR imaging. ACS Appl Mater Interfaces. 2020;12(10):12143–54.
[40] Zheng XH, Wang LL, Zheng MZ, Zhong JJ, Chen YY, Shen YL. RGFP966 inactivation of the YAP pathway attenuates cardiac dysfunction induced by prolonged hypothermic preservation. J Zhejiang Univ Sci B. 2020;21(9):703–15.
[41] Guo Y, Wang XY, Chen YL, Liu FQ, Tan MX, Ao M, et al. A light-controllable specific drug delivery nanoplatform for targeted bimodal imaging-guided photothermal/chemo synergistic cancer therapy. Acta Biomater. 2018;80:308–26.
[42] Wang Z, Ding J, Ma X, Luo S. Selective ultrasound contrast enhancement in the tumor by nanocapsules with perfluorooctylbromide: Effect of PLGA-PEG proportion. RSC Adv. 2018;8(32):17958–66.
[43] Waters ES, Kaiser EE, Yang X, Fagan MM, Scheulin KM, Jeon JH, et al. Intracisternal administration of tanshinone IIA-loaded nanoparticles leads to reduced tissue injury and functional deficits in a porcine model of ischemic stroke. IBRO Neurosci Rep. 2021;10:18–30.
[44] Wang L, Xu L, Du J, Zhao X, Liu M, Feng J, et al. Nose-to-brain delivery of borneol modified tanshinone IIA nanoparticles in prevention of cerebral ischemia/reperfusion injury. Drug Deliv. 2021;28(1):1363–75.
[45] Wang H, Zhong L, Mi S, Song N, Zhang W, Zhong M. Tanshinone IIA prevents platelet activation and down-regulates CD36 and MKK4/JNK2 signaling pathway. BMC Cardiovasc Disord. 2020;20(1):81.
[46] Guo R, Li L, Su J, Li S, Duncan SE, Liu Z, et al. Pharmacological activity and mechanism of tanshinone IIA in related diseases. Drug Des Dev Ther. 2020;14:4735–48.
[47] Kal A, Kal O, Akillioglu I, Celik E, Yilmaz M, Gonul S, et al. The protective effect of prophylactic ozone administration against retinal ischemia-reperfusion injury. Cutan Ocul Toxicol. 2017;36(1):39–47.
[48] Cai HA, Tao X, Zheng LJ, Huang L, Peng Y, Liao RY, et al. Ozone alleviates ischemia/reperfusion injury by inhibiting mitochondrion-mediated apoptosis pathway in SH-SY5Y cells. Cell Biol Int. 2020;44(4):975–84.
[49] Wei H, Chen J, Wang S, Fu F, Zhu X, Wu C, et al. A nanodrug consisting of doxorubicin and exosome derived from mesenchymal stem cells for osteosarcoma treatment in vitro. Int J Nanomed. 2019;14:8603–10.
[50] Zhang BP, Qiu H, Wang DW, Liu YQ, Bi ZG. Improved blood compatibility of Mg-1.0Zn-1.0Ca alloy by micro-arc oxidation. J Biomed Mater Res Part A. 2011;99(2):166–72.
[51] Luo M, Lewik G, Ratcliffe JC, Choi CHJ, Makila E, Tong WY, et al. Systematic evaluation of transferrin-modified porous silicon nanoparticles for targeted delivery of doxorubicin to

glioblastoma. ACS Appl Mater Interfaces. 2019;11(37):33637–49.
[52] Cui X, Song K, Lu X, Feng W, Di W. Liposomal delivery of MicroRNA-7 targeting EGFR to inhibit the growth, invasion, and migration of ovarian cancer. ACS Omega. 2021;6(17):11669–78.
[53] Zhou L, Zhang J, Wang C, Sun Q. Tanshinone inhibits neuronal cell apoptosis and inflammatory response in cerebral infarction rat model. Int J Immunopathol Pharmacol. 2017;30(2):123–9.
[54] Hua Y, Li C, Hu J, Wang YY, Liu PL, Gao BY, et al. Fluoxetine adjunct to therapeutic exercise promotes motor recovery in rats with cerebral ischemia: Roles of nucleus accumbens. Brain Res Bull. 2019;153:1–7.
[55] Chopra A. ZW800-1, a zwitterionic near-infrared fluorophore, and its cyclic RGD peptide derivative cyclo-(RGDyK)-ZW800-1. Molecular Imaging and Contrast Agent Database (MICAD). Bethesda (MD); 2004.
[56] Palchetti S, Colapicchioni V, Digiacomo L, Caracciolo G, Pozzi D, Capriotti AL, et al. The protein corona of circulating PEGylated liposomes. Biochim Biophys Acta. 2016;1858(2):189–96.
[57] Blanco-Colino R, Espin-Basany E. Intraoperative use of ICG fluorescence imaging to reduce the risk of anastomotic leakage in colorectal surgery: A systematic review and meta-analysis. Tech Coloproctol. 2018;22(1):15–23.
[58] Bhavane R, Starosolski Z, Stupin I, Ghaghada KB, Annapragada A. NIR-II fluorescence imaging using indocyanine green nanoparticles. Sci Rep. 2018;8(1):14455.
[59] Urade T, Sawa H, Iwatani Y, Abe T, Fujinaka R, Murata K, et al. Laparoscopic anatomical liver resection using indocyanine green fluorescence imaging. Asian J Surg. 2020;43(1):362–8.
[60] Chan PS, Xian JW, Li Q, Chan CW, Leung SSY, To KKW. Biodegradable thermosensitive PLGA-PEG-PLGA polymer for non-irritating and sustained ophthalmic drug delivery. AAPS J. 2019;21(4):59.
[61] Vojtova L, Michlovska L, Valova K, Zboncak M, Trunec M, Castkova K, et al. The effect of the thermosensitive biodegradable PLGA(-)PEG(-)PLGA copolymer on the rheological, structural and mechanical properties of thixotropic self-hardening tricalcium phosphate cement. Int J Mol Sci. 2019;20(2):391.
[62] Xiao B, Chai Y, Lv S, Ye M, Wu M, Xie L, et al. Endothelial cell-derived exosomes protect SH-SY5Y nerve cells against ischemia/reperfusion injury. Int J Mol Med. 2017;40(4):1201–9.
[63] Kadari A, Pooja D, Gora RH, Gudem S, Kolapalli VRM, Kulhari H, et al. Design of multifunctional peptide collaborated and docetaxel loaded lipid nanoparticles for antiglioma therapy. Eur J Pharm Biopharm: Official J Arbeitsgemeinschaft fur Pharmazeutische Verfahrenstechnik eV. 2018;132:168–79.
[64] Sardi I, Fantappie O, la Marca G, Giovannini MG, Iorio AL, da Ros M, et al. Delivery of doxorubicin across the blood-brain barrier by ondansetron pretreatment: A study in vitro and in vivo. Cancer Lett. 2014;353(2):242–7.
[65] Lv W, Xu J, Wang X, Li X, Xu Q, Xin H. Bioengineered boronic ester modified dextran polymer nanoparticles as reactive oxygen species responsive nanocarrier for ischemic stroke treatment. ACS Nano. 2018;12(6):5417–26.
[66] Ansari MA, Khan FB, Safdari HA, Almatroudi A, Alzohairy MA, Safdari M, et al. Prospective therapeutic potential of Tanshinone IIA: An updated overview. Pharmacol Res. 2021;164:105364.
[67] Sun G, Sun K, Sun J. Combination prostate cancer therapy: Prostate-specific membranes antigen targeted, pH-sensitive nanoparticles loaded with doxorubicin and tanshinone. Drug Deliv. 2021;28(1):1132–40.
[68] Martins C, Sarmento B. Microfluidic manufacturing of multi-targeted PLGA/PEG nanoparticles for delivery of taxane chemotherapeutics. Methods Mol Biol. 2020;2059:213–24.
[69] Chen F, Zhang J, He Y, Fang X, Wang Y, Chen M. Glycyrrhetinic acid-decorated and reduction-sensitive micelles to enhance the bioavailability and anti-hepatocellular carcinoma efficacy of tanshinone IIA. Biomater Sci. 2016;4(1):167–82.
[70] Giraudeau C, Moussaron A, Stallivieri A, Mordon S, Frochot C. Indocyanine green: Photosensitizer or chromophore? Still a debate. Curr Med Chem. 2014;21(16):1871–97.
[71] Wei X, Zhan C, Chen X, Hou J, Xie C, Lu W. Retro-inverso isomer of Angiopep-2: A stable d-peptide ligand inspires brain-targeted drug delivery. Mol Pharm. 2014;11(10):3261–8.
[72] Rahman M, Sharma G, Thakur K, Goni VG, Katare OP, Anwar F, et al. Emerging advances in nanomedicine as a nanoscale pharmacotherapy in rheumatoid arthritis: State of the art. Curr Top Med Chem. 2016;17(2):162–73.
[73] Rizvi SAA, Saleh AM. Applications of nanoparticle systems in drug delivery technology. Saudi Pharm J. 2018;26(1):64–70.
[74] Swider E, Koshkina O, Tel J, Cruz LJ, de Vries IJM, Srinivas M. Customizing poly(lactic-*co*-glycolic acid) particles for biomedical applications. Acta Biomater. 2018;73:38–51.
[75] Wu D, Zhao Z, Wang N, Zhang X, Yan H, Chen X, et al. Fluorescence imaging-guided multifunctional liposomes for tumor-specific phototherapy for laryngeal carcinoma. Biomater Sci. 2020;8(12):3443–53.
[76] Yang G, Lv R, Gai S, Dai Y, He F, Yang P. Multifunctional SiO2@Gd2O3:Yb/Tm hollow capsules: controllable synthesis and drug release properties. Inorg Chem. 2014;53(20):10917–27.
[77] You Q, Sun Q, Wang J, Tan X, Pang X, Liu L, et al. A single-light triggered and dual-imaging guided multifunctional platform for combined photothermal and photodynamic therapy based on TD-controlled and ICG-loaded CuS@mSiO2. Nanoscale. 2017;9(11):3784–96.
[78] Tan X, Wang J, Pang X, Liu L, Sun Q, You Q, et al. Indocyanine green-loaded silver nanoparticle@polyaniline core/shell theranostic nanocomposites for photoacoustic/near-infrared fluorescence imaging-guided and single-light-triggered photothermal and photodynamic therapy. ACS Appl Mater Interfaces. 2016;8(51):34991–5003.
[79] Yoo SJ, Cho B, Lee D, Son G, Lee YB, Soo Han H, et al. The erythropoietin-derived peptide MK-X and erythropoietin have neuroprotective effects against ischemic brain damage. Cell Death Dis. 2017;8(8):e3003.
[80] Israel LL, Braubach O, Galstyan A, Chiechi A, Shatalova ES, Grodzinski Z, et al. A combination of tri-leucine and angiopep-2 drives a polyanionic polymalic acid nanodrug platform across the blood-brain barrier. ACS Nano. 2019;13(2):1253–71.
[81] Shao K, Huang R, Li J, Han L, Ye L, Lou J, et al. Angiopep-2 modified PE-PEG based polymeric micelles for amphotericin B delivery targeted to the brain. J Control Rel. 2010;147(1):118–26.
[82] Piccolo MT, Menale C, Crispi S. Combined anticancer therapies: An overview of the latest applications. Anticancer Agents Med Chem. 2015;15(4):408–22.